Fabrication of silicon molds with multi-level, non-planar, micro- and nano-scale features

2014 Nanotechnology 25 375301

(http://iopscience.iop.org/0957-4484/25/37/375301)

IOP Publishing Nanotechnology
Nanotechnology **25** (2014) 375301 (11pp) doi:10.1088/0957-4484/25/37/375301

Fabrication of silicon molds with multi-level, non-planar, micro- and nano-scale features

S Azimi[1,2], Z Y Dang[1], K Ansari[3] and M B H Breese[1,2]

[1] Department of Physics, National University of Singapore, Singapore 117542, Singapore
[2] Singapore Synchrotron Light Source (SSLS), National University of Singapore, 5 Research Link, Singapore 117603, Singapore
[3] Institute of Materials Research and Engineering (IMRE), 3 Research Link, Singapore 117602, Singapore

E-mail: phymbhb@nus.edu.sg

Received 25 April 2014, revised 25 June 2014
Accepted for publication 25 June 2014
Published 22 August 2014

Abstract

A method for single-step fabrication of arbitrary, complex, three-dimensional (3D) silicon structures from the nano- to millimeter-scale at multiple levels on non-planar, curved, or domed surfaces is reported. The fabrication is based on focused or masked ion beam irradiation of p-type silicon followed by electrochemical anodization. The process allows fabrication of a wide range of surface features at multiple heights and with arbitrary orientations by varying the irradiated feature width, ion type, energy fluence, and subsequent anodization conditions. The technology has achieved depth resolution of 10 nm as step heights and is capable of creating lateral features down to 7 nm at high aspect ratios of up to 40, with surface roughness down to 1 nm scaled up to full wafer areas. The single-step ability has seamlessly interfaced a network of complex, integrated micro- to nano-structures in 3D orientations with no alignment required. The final template has been converted to a master copy for nano-imprinting lithography of 3D fluidic structures and optical components.

Keywords: silicon micromachining, micro- and nano-patterning, nano-lithography, three-dimensional mold, electrochemical anodization

(Some figures may appear in colour only in the online journal)

1. Introduction

Researchers utilize nano-fabrication to confine biological, physical, and chemical systems at molecular and ionic levels to accurately manipulate physical and chemical variables. A combination of complex, three-dimensional (3D) micro- and nano-scale structures on the surface of materials create advanced properties and functionalities with numerous applications. For example, the cuticle texture on terrestrial plants, particularly lotus leaves, form a hydrophobic self-cleaning surface and, inspired by nature, similar structures fabricated by patterning techniques also produce a super-hydrophobic water-repellent surface [1–3]. Butterfly wings exhibit structural colors arising from their natural self-assembled, multi-level, 3D nano-structures [4]. Such biological nano-structures are ideal examples of photonic crystals, which have inspired the design and fabrication of new photonic structures, and also serve directly as bio-templates to mimic those structures. 3D multilevel surface topography has exhibited anti-bacterial [5–7] and anti-fouling surface properties [3]. The growing field of mechanobiology utilizes 3D synthesized topographies for the study and manipulation of cells and DNA for diagnostic applications [8–12] and 3D hierarchical structures exhibit a large surface area, providing the possibility of achieving useful functionalities for applications in sensors with enhanced sensitivity for biomolecules [13] or improved electrochemical sensitivity and detection limit for analyzes and catalysts [14]. Enhanced light absorption leads to improved photonics and optical components [15] and as electrodes to create larger areas as super-capacitors for fuel cells [16]. A large surface contact leads to enhanced surface adhesion similar to a gecko's foot [17], or to reduced drag force due to an air/liquid interface which is similar to shark skin [18]. Tissue engineering has utilized 3D micro-fabrication to create templates for casting materials as scaffolds with capillary networks such as biodegradable

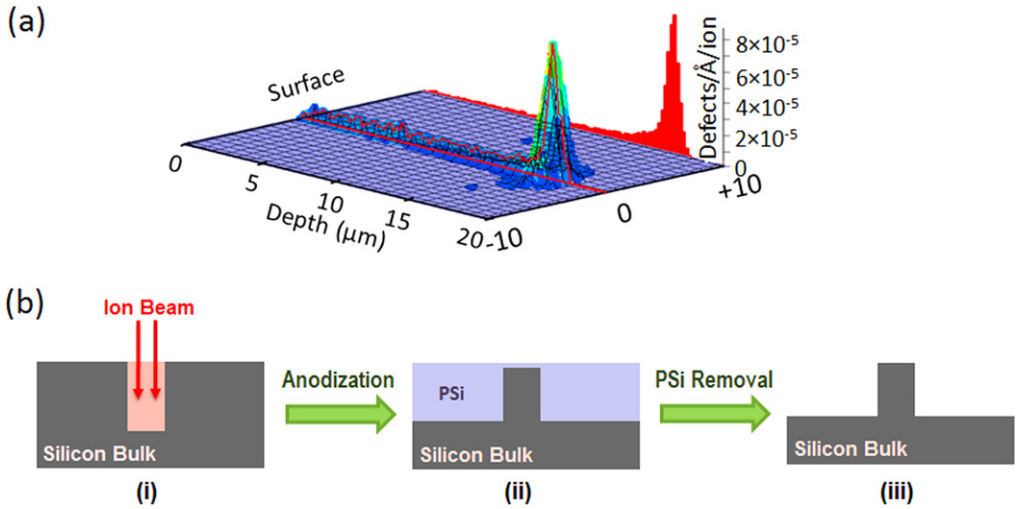

Figure 1. (a) SRIM (stopping and range of ions in matter) [58, 59] plot of the defect distribution versus depth for 1 MeV protons in silicon, within a box size of $20 \times 20\,\mu$m. (b) Schematics of the silicon mold fabrication process based on ion beam irradiation and electrochemical anodization.

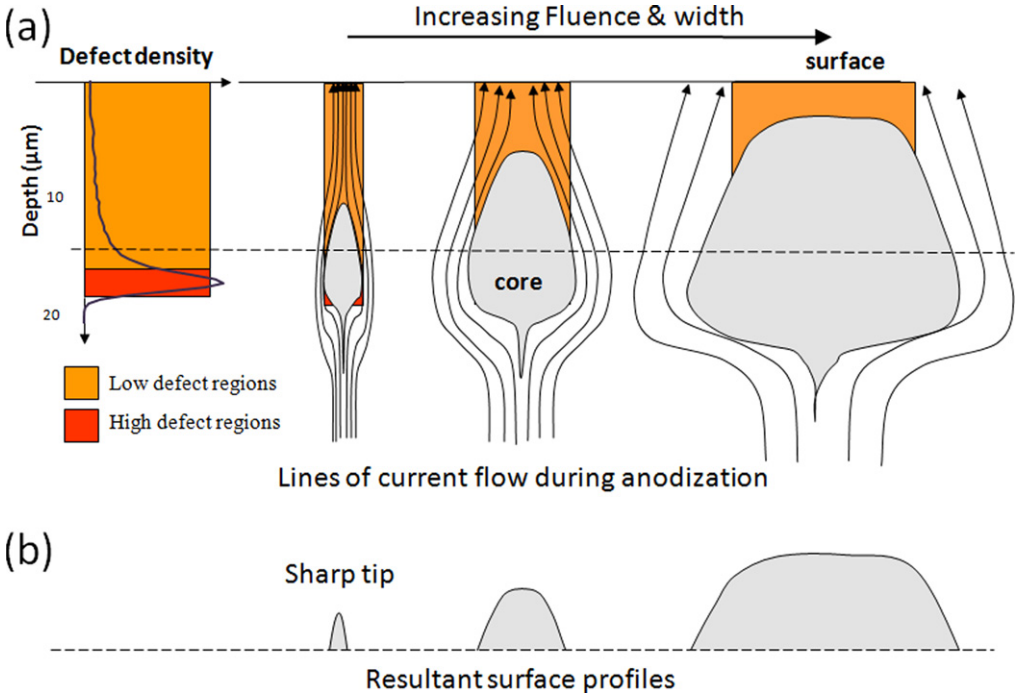

Figure 2. (a) Schematic of the electrochemical anodization process where end-of-range regions remain as a solid silicon core, where those regions closer to the surface are anodized. For higher fluences, the surface regions also remain unanodized. (b) By varying the fluence and irradiated width, and controlling the etch depth a variety of feature heights and geometries are produced.

hydrogels containing microfabricated blood vessels that mimic the real human body tissue that have recently been used in real applications for transplantable body tissues [19–24].

Despite numerous efforts, 3D nano-fabrication at multi-scales of height and lateral dimensions remains highly challenging, both in terms of techniques and processes as well as patterning materials [25]. To date the fabrication techniques are either based on self-assembly or direct write and essentially all of them are two-dimensional, or if 3D, the patterns only lie on a single plane and/or a non-curved, flat surface consisting of low to high resolutions but of similar heights. Self-assembly based approaches rely on a thermodynamic balance between entropically- and enthalpically-driven molecular forces to produce ordered domains [26, 27]. Direct write techniques which are capable of fabricating 3D nano-structures can be summarized as: phase mask lithography [28–30] and multi-beam holography (also known as interference lithography) [31, 32] which both rely on exposure through a pre-patterned transparent mold/mask and therefore their resolution are limited by the mask patterns, use of conventional semiconductor manufacturing techniques [33],

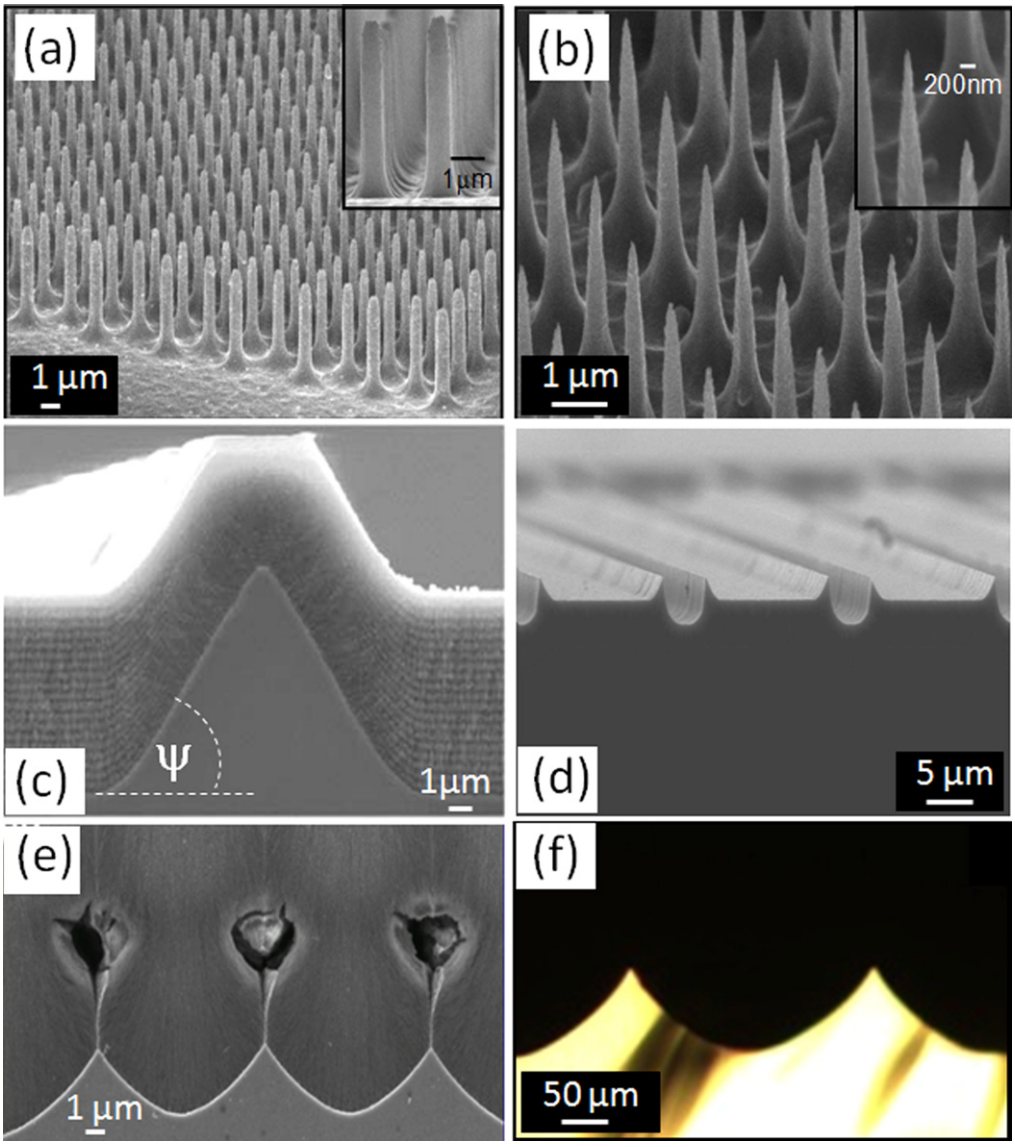

Figure 3. Cross-section and plan view SEM images of surface machined profiles produced by 2 MeV proton irradiation of 0.02 Ω cm p-type silicon. (a), (b) High aspect pillars and spikes. (c) Cross-section SEM image of a 6 μm wide region irradiated with a fluence of 4×10^{15} cm^{-2}. (d) Sharp ridges. (e), (f) respectively show cross-sectional electron/optical micrographs of a concave surface profile.

techniques for 3D printing by FIB implantation and layer deposition [34] and techniques using laser irradiation and etching of glass [35]. Two photon lithography [36–39] has a 3D high resolution capability but only on planar surfaces and the resolution especially in height is highly dependent on the photo-polymerization initiators [40, 41]. Currently, there is no lithography technique that can fabricate these structures in a single step.

Mold technology is a simple solution to this challenge. When combined with nano-imprint lithography [42–45], hot embossing [46] or nano-injection molding [47], it leads to a high resolution nano-fabrication technique which can create structures down to sub-10 nm resolution [48] over large areas in a single step and into different materials with a flexibility and functionality that is easily accessible to users. There have been attempts to use mold technology for 3D patterning such as reversal imprinting [49–51], dissolvable molds [52] and microcontact printing using a soft mold [53]. To extend the capability of mold technology to 3D fabrication at multiple levels and/or non-planar surfaces with arbitrary directions, there are two major obstacles. One is on the limitation of patterning in space orientations either in resolution or in dimensional aspects. The second difficulty is the seamless interface issue which at 3D becomes a challenge both for connecting micro- and nano-structures in 3D space orientations at different heights and constructing the connections to the outside world [51, 52].

This paper describes a method of fabricating a high-quality master containing different scales of features on its surface with feature resolution down to 10 nm over large areas on a silicon substrate. The master can be converted to a metal replica utilizing standard metal electroplating. Our single, integrated process allows fabrication of machined silicon surfaces with the following characteristics: (i)

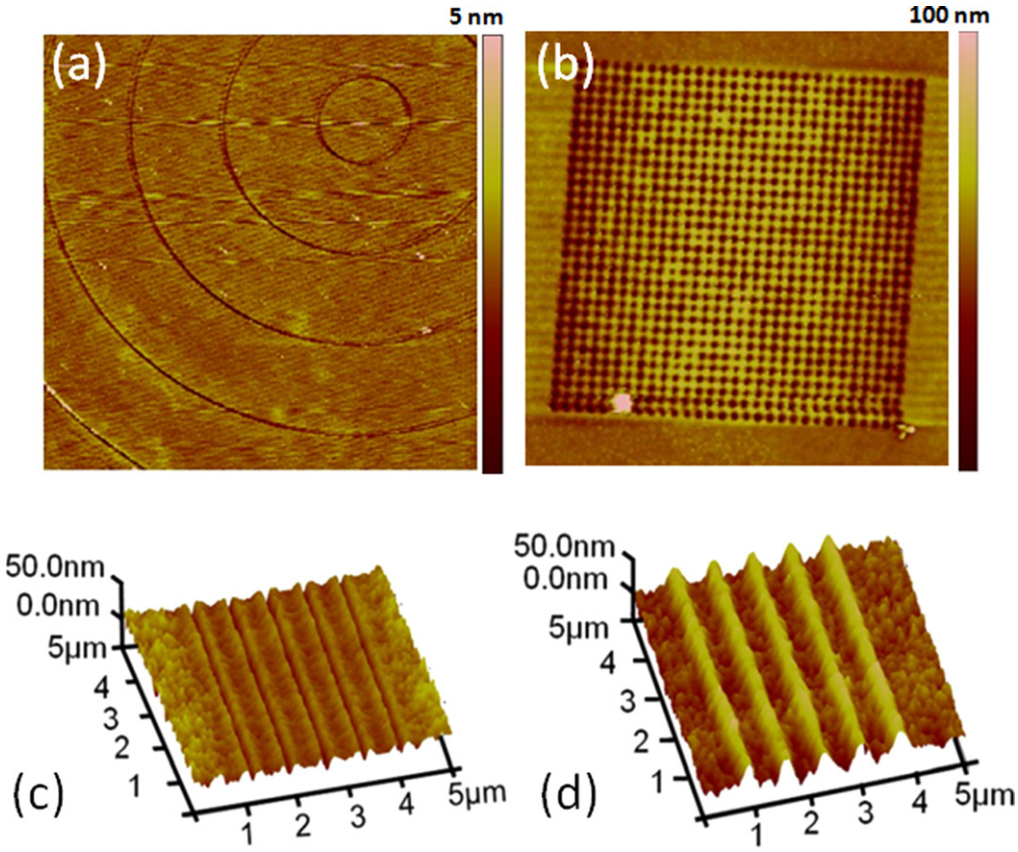

Figure 4. AFM images of point and line irradiations using 30 keV helium ions, focused to ∼1 nm. (a) Chemical etching only, (b) to (d) after electrochemical anodization and oxidation smoothening. In (b) the dot period is 200 nm. (c), (d) respectively show the effects of a low/high fluence.

combined micro-scale and nano-scale patterning, both laterally and in depth, (ii) high and/or low aspect ratio features which can be rectilinear or any other shape such as triangular, conical, convex/concave, aligned in any arbitrary direction, (iii) smooth surfaces where the roughness can be controlled down to a 1 nm, (iv) either maskless irradiation using direct writing for great flexibility over small areas, or an extension of the process to large areas for commercially viable quantities using masked irradiation in conjunction with UV lithography, (v) easy integration with mold and imprinting for mass production.

2. Underlying physical science

The basic science underlying our silicon surface machining process involves high-energy ion beam irradiation of p-type wafers, followed by electrochemical anodization, as shown in figures 1, 2. Irradiation with light ions such as protons and helium ions of high and low energies, causes crystalline damage to silicon, mostly as vacancy-interstitial pairs but also a range of other defect types and effects on the motion of charge carriers [54–57]. The defect production rate of such high-energy light ions with energies greater than about 50 keV, peaks close to their end-of-range depth [58, 59], which, for the example considered of 1 MeV protons in figure 1(a), is around 15 μm. A high ion fluence produces a high density of defects which locally reduce the free carrier density, so increasing the resistivity along the full irradiated trajectory [60, 61]. A high fluence typically results in a reduction of the electrical hole current flowing through irradiated regions during subsequent electrochemical anodization [62, 63], slowing down or completely stopping porous silicon formation, leaving unetched fully crystalline regions completely surrounded by porous silicon if anodization proceeds beyond the end-of-range [64]. The underlying silicon structure may be revealed by removing the porous silicon with potassium hydroxide (KOH), figure 1(b). A micromachining process using this principle has been developed and used to fabricate a range of patterned 3D microstructures in silicon and other semiconductors [64–67]. If anodization is stopped before the end-of-range depth then the silicon surface may be patterned with a wide range of feature widths and heights, figure 2(b).

3. Fabrication of complex silicon molds

In order to combine surface features which are patterned on both a nano- and micro-scale, the critical fabrication step is the ability to combine high and low fluence irradiations into the same process, and an understanding of the effect of a

given fluence on the anodized surface relief. In the case of direct writing using a high-energy ion beam in a nuclear microprobe [68], irradiation is performed by scanning a focused beam current of 10–100 pA a single time over areas where low fluences are required, while scanning the same beam many times over areas where higher fluences are required. In this way, variations in fluence from 10^{13} to 10^{16} ions cm^{-2} are delivered within the scanned area. At a low fluence irradiated line, porous silicon is formed at the surface, and only closer to the end-of-range does the defect density become high enough to stop anodization and allow the formation of a narrow tip at the top of the end-of-range core, figure 2(b). Thus if the anodization is stopped just when the tip of the core is exposed, a triangular protuberance is formed. The choice of different irradiation geometries and fluences up to 10^{16} ions cm^{-2} allow the fabrication of pillars and spikes in figures 3(a), (b) and sharp ridges in figures 3(c), (d) in 0.02 Ω cm silicon.

In wide irradiated regions, anodization may be completely stopped with a high fluence, or for lower fluences the etch rate is slowed down in proportion to the fluence, allowing precisely controlled step heights and angled surfaces to be machined [69, 70]. In such cases, the anodized surface may have a flat top or a triangular profile, depending on the ion energy and fluence used for irradiation. In figure 3(c) a proton fluence of 4×10^{15} cm^{-2} was used to irradiate a 6 μm wide region. The sample was anodized to a depth of 12 μm, then the porous silicon removed, see the upper layer profile which shows a flat top with tilted sidewalls to either side. The fluence is high enough to slow down the rate of anodization by about 50%, resulting in a flat-topped region which is about 6 μm higher than the surrounding unirradiated surface. On further anodization a triangular profile is formed by continued anodization when the opposing sidewalls meet, see lower silicon profile, where the boundary tilt angle ψ increases with anodization depth and fluence, allowing a wide range of tilts to be controllably produced. Figures 3(e), (f) show concave surface profiles produced by a slight modification of the same process; these examples show how the radius of curvature can be varied from about 100 μm down to about 3 μm.

Figure 4 shows surface patterning of silicon using a similar ion beam irradiation and etching process, where high resolution surface patterning is achieved. Irradiations were performed with 30 keV helium ions focused to a spot size of 1 nm in a Helium Ion Microscope. The spectrum of defects created is the same as that for high energy light ion irradiation, the only difference being that the defects are created much closer to the surface and with little lateral beam spread, allowing high resolution patterning. In figure 4(a), the irradiated wafer was chemically etched in 2% HF for 8 mins, and 24% HF for 2 mins. The irradiated regions are slowly dissolved away while the unirradiated surface is unaffected. The full-width-at-half-maximum of the resulting dips is about 30 nm, and their depth in this example is about 2 nm. In the rest of figure 4 the irradiated wafer was electrochemically anodized in 24% HF for few seconds at 60 mA cm^{-2}, and then smoothened via thermal oxidation at 700 ~ 1000 °C for 20 mins, and oxide removed in 2% HF. The electrochemical anodization time was 3 s in each case. Using this mode of irradiation, one can choose whether the resulting feature height of tens of nano-meters should be a protruding point/ridge standing above the surrounding unirradiated surface, as in figure 2, or a dip, depending on the fluence and the anodization conditions [60], providing another degree of flexibility to the final patterned surface.

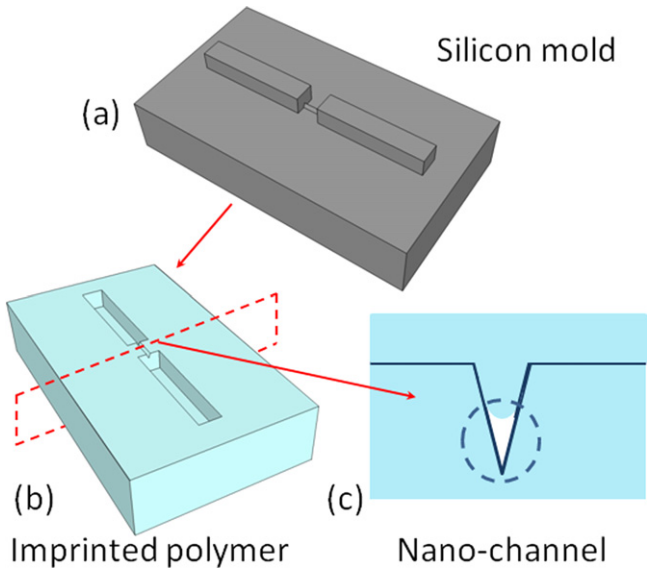

Figure 5. Schematic fabrication of combined micro-/nano-scale patterning of (a) silicon surface showing two long microchannels with a nano-scale channel running between them, (b) after imprinting this surface to form an inverse copy and (c) how this inverse pattern can be used to form a nano-scale channel by imprinting it again with a soft polymer which partially fills the triangular base.

Examples are described in the following section which demonstrate the use of this silicon surface machining process for nano-imprinting. The first example shows how to combine micro- and nano-scale channels in a surface mold for subsequent stamping/reproducing fluidic devices which also incorporate large-scale components for connecting to the outside world. The second example describes how to fabricate precisely-controlled, smooth, four-level surfaces on silicon for stamping into a transparent polymer for optics applications. A third example shows how different length and height scales of patterning can be integrated to produce hierarchical patterning over micrometer to nano-meter feature dimensions.

4. Combined micro- and nano-scale channels for microfluidics

Figure 5(a) shows a schematic in which two widely differing ion fluence irradiations are used to form a nano-ridge (low fluence, narrow line irradiation) which is connected to long micro-ridges (high fluence, wide area irradiation). The micro-ridges can be of any length, and connected to larger-scale components which are either direct-written in the same manner, or the process can be extended to patterning large surfaces using a mode of irradiation which delivers a highly-

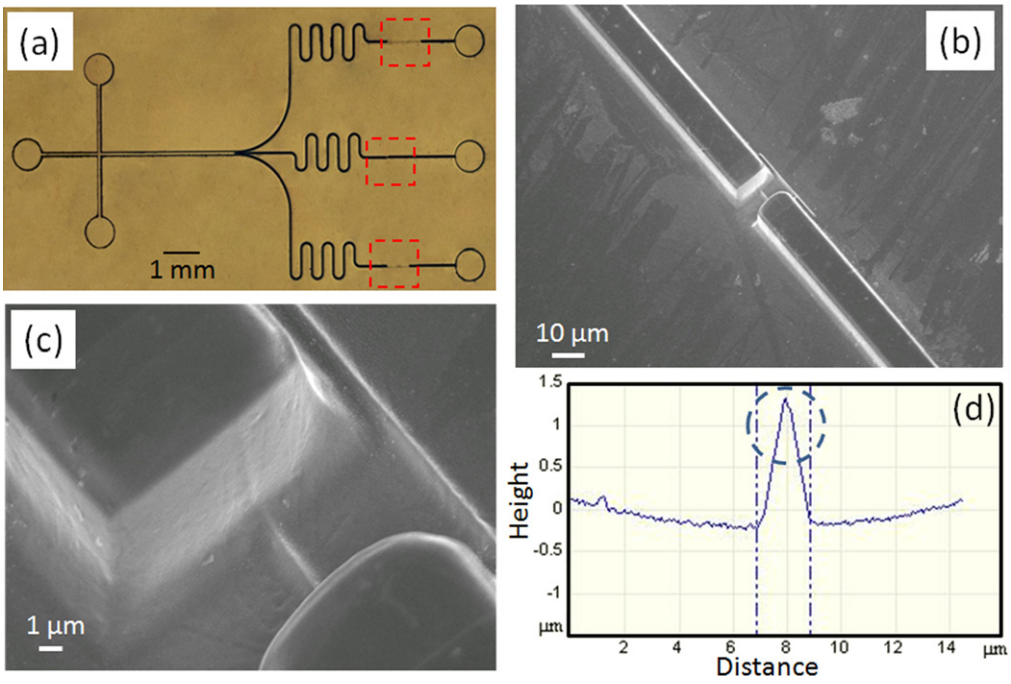

Figure 6. (a) Low magnification optical micrograph of RIE patterned silicon surface, with gaps left for fabrication of nano-channels at locations within the dashed boxes. (b), (c) SEMs showing silicon surface micro-ridges connected by a nano-ridge. (d) AFM line profile across the nano-ridge.

uniform beam fluence over areas of many square centimeters in a short time [70]. The next process stage, figure 5(b), involves using the patterned silicon surface as a mold for imprinting the pattern into a polymer such as polycarbonate (PC), to form an inverse copy. Figure 5(c) shows how this inverse pattern is used to form a nano-scale channel by imprinting it again into a soft polymer which partially fills the triangular base, leaving the narrow apex clear for fluidic flow.

Figure 6(a) shows another mode of how this process can be combined with conventional wafer patterning to form a large area surface comprising features which are patterned with different widths and heights ranging from tens of microns to hundreds of nano-meters. The large-scale features of a microfluidic device were patterned using reactive ion etching (RIE), to a depth of a few micrometers. Our direct-write nano-scale patterning process was then applied to the pre-patterned silicon surface in which suitable gaps had been left to incorporate such nano-channels, see dashed boxes in figure 6(a). Figures 6(b), (c) show a micrometer-length nano-ridge (created using a 1 MeV proton low fluence of 5×10^{15} cm^{-2}, narrow line irradiation) connecting two long micro-ridges which have a width of 10 μm. The AFM profile in figure 6(d) was recorded across the spare channel shown in figure 6(c), which was created for this purpose. The nano-ridge is about 1.5 μm in height has a symmetric profile.

Prior to imprinting, the silicon mold was treated with 1H,1H,2H,2H perfluorodecyltrichlorosilane for hydrophobic surface treatment to obtain a fluorinated self-assembled monolayer with a very low surface energy. Imprinting was carried out with a commercial nano-imprinter using 125 μm thick sheets of PC as a polymeric substrate. The PC film was imprinted at 170 °C and 50 bars of pressure for 400 s.

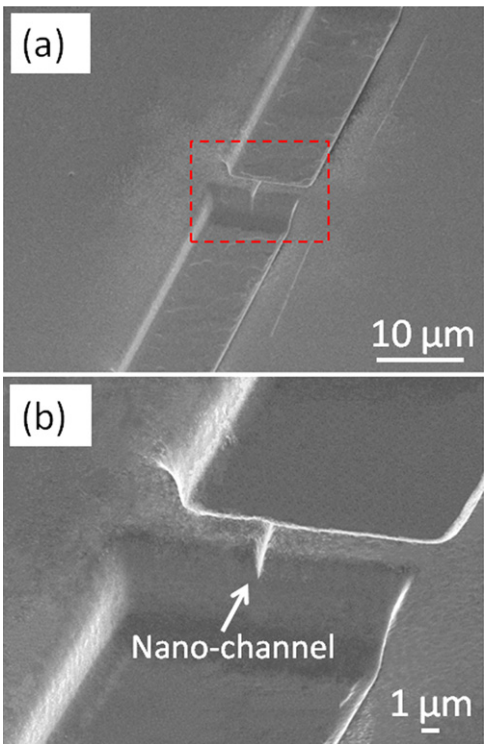

Figure 7. Micro-/nano-scale patterns imprinted into PC.

Figure 7 shows imprinted copies of the nano-ridge, which is ~0.4 μm wide at its base and 1 μm deep. From this one can deduce an apex angle of ~25°, showing that it is indeed a sharply imprinted feature.

5. Precisely controlled surface steps for phase plates

The same machining process described above may be used to fabricate a range of precisely controlled surface step heights to give a large-area pattern of four-level surfaces which can be imprinted to a transparent polymer. Each group of four-level sub-pixels comprises a 'super-pixel', with the pattern repeated over a surface area of many square centimeters. In optics, this may be used for 3D imaging by placing the transparent sheet in front of a CCD camera. The four sub-pixels act as phase plates to manipulate the imaginary part of the incident laser beam, resulting in interference with adjacent sub-pixels in two different directions.

While the previous example of combining micro/nano-scale channels used direct writing to achieve different fluences, here we use a large area irradiation mode which allows rapid patterning using a highly-uniform beam fluence, which

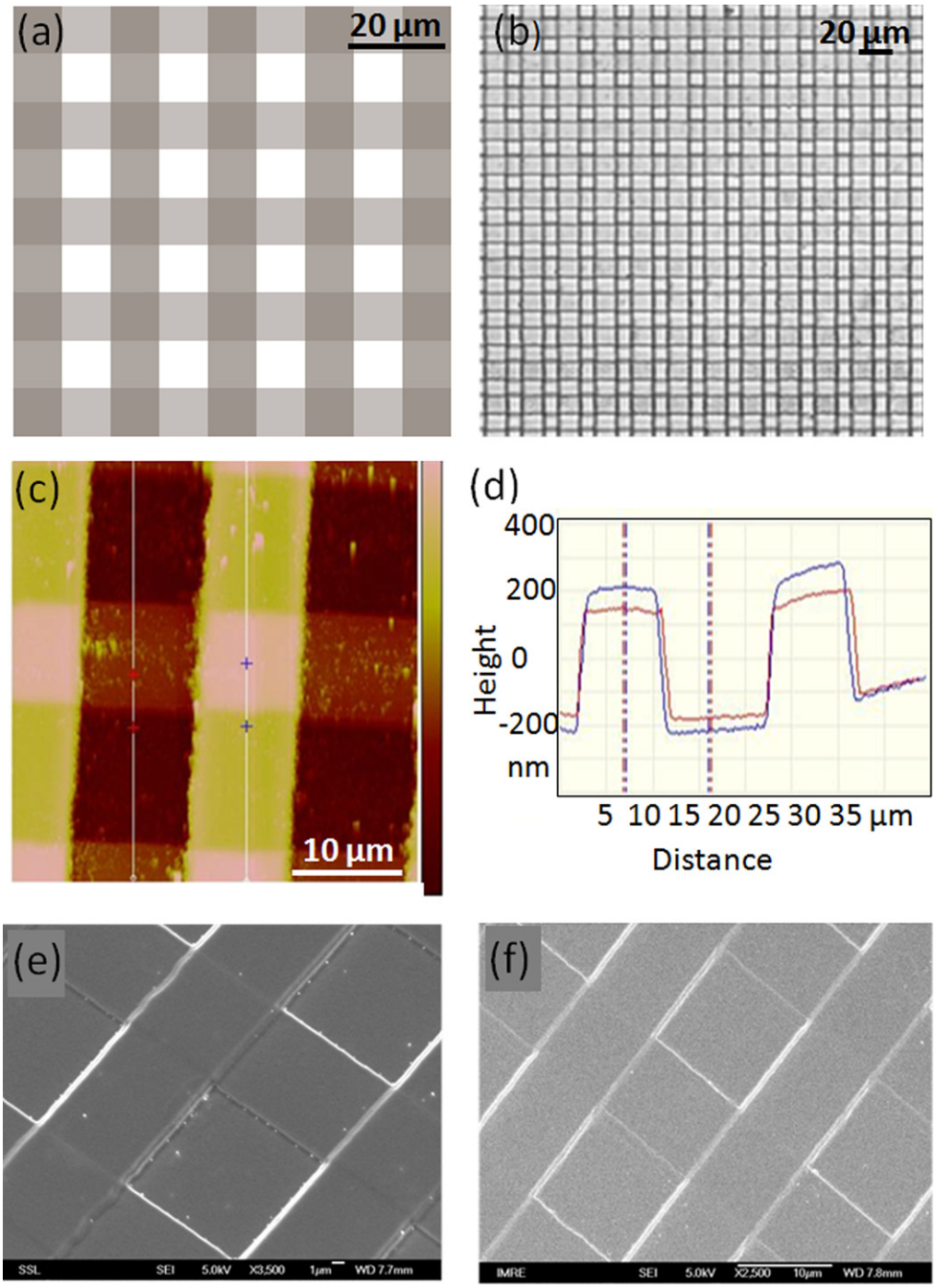

Figure 8. (a) Schematic of the irradiation process for fabricating a surface relief pattern of squares of four different heights, created using large area irradiation with different 1 MeV proton fluences in orthogonal directions. (b) Optical micrograph after anodization and (c) AFM image of surface relief pattern of 10 μm squares after anodization. (d) AFM line scans of patterned surface after thermal annealing. (e) SEM image of the machined four level silicon surface and (f) PC surface after nano-imprinting.

is ideally suited to fabricating shallow, smooth surface steps. The wafer was first coated with a 5 μm thick SU-8 photoresist layer, and patterned with 10 μm wide lines and spaces using standard UV photolithography, see horizontal lines in figure 8(a). The sample was then irradiated with a 200 keV proton fluence of 5×10^{14} cm^{-2}. These ions have a range of ~2 μm in SU-8, so they are completely stopped. After irradiation the resist is removed, and the second resist lines with the same dimensions are patterned orthogonal to the previous direction using a similar UV lithography step, see vertical lines in figure 8(a). The sample was then irradiated again with a 200 keV proton fluence of 1×10^{15} cm^{-2}, giving an array of unirradiated squares together with three adjacent squares which are irradiated with fluences of 0.5, 1.0 and 1.5×10^{15} protons cm^{-2}. During anodization, the different irradiated regions progressively slow down the porous silicon formation rate, figure 3(e); the lowest and highest regions are respectively produced at unirradiated and the highly-irradiated areas. Figure 8(b) shows an optical micrograph of the four-level patterned surface after electrochemical anodization at 90 mA cm^{-2} for 10 s and removal of the porous silicon.

In the AFM image in figure 8(c) the silicon surface appears rough due to several factors. First the anodized surface of silicon has a natural roughness associated with it, owing to the random nature of pore formation. The standard process to reduce surface roughness is thermal oxidation [71, 72]. A second source of roughness is a layer of low porosity silicon clinging to the anodized surface even after immersion in KOH, which makes the visible surface much rougher that the underlying crystalline surface. Third, the presence of small chunks of porous silicon sticking to the surface which are difficult to remove. We consider thermal oxidation to be the most effective way of minimizing all these sources of roughness; after annealing for 2 h at 1100 °C and removing the resultant oxide layer using dilute HF solution, the AFM linescan in figure 8(d) exhibits a smooth surface profile. The final surface roughness produced by our fabrication process followed by thermal oxidation is as low as 1 nm. The patterned surface was then imprinted in a similar manner as described above. Figures 8(e), (f) respectively show SEMs of the four-level patterned surface in silicon and after imprinting in PC, from which the good reproduced quality is clear.

This example shows how step heights of a few hundred nano-meters are formed and transferred to a polymer copy. By carefully controlling the fluences used for irradiation and also using a shallower anodization depth, smaller step heights can be machined using this process. Figure 9 shows a single step height of ~10 nm produced in this fashion using 1 MeV proton irradiation with slightly differing fluences of 1×10^{15} cm^{-2} and 1.1×10^{15} cm^{-2} and anodized at 90 mA cm^{-2}.

A major strength of our approach to patterning lies in the ability to integrate features of different dimensions in length and height into a *hierarchical* structure. The above work on integrating micro- and nano-channels provided one example of this. Other examples are given in figures 10(a), (b), which shows examples of $50\times50\,\mu$m^2 areas comprising two

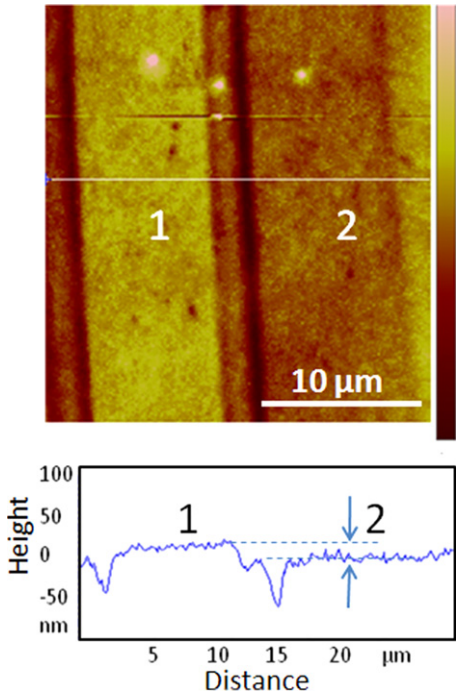

Figure 9. AFM image (top) and (bottom) line scan after thermal annealing, showing a step height of ~10 nm between two 10 μm wide surfaces, produced using two slightly differing fluences.

different types of patterns, made with proton beam irradiation using 250 keV protons. The $10\times10\,\mu$m^2 squares are 1 μm in height in both examples whereas the fine-scale array of dots are of different heights. One can choose to pattern the surface with uniform height features, or vary the height simply by altering the proton fluence at each point. In (c), a fine-scale pattern covers the entire surface, encompassing both the raised and lower surface of the coarser-scale pattern.

6. Conclusions

We have developed a method for single-step fabrication of arbitrary, complex, 3D silicon structures from the nano- to millimeter-scale at multiple levels and non-planar, curved, or domed surfaces. Multistep surfaces can be combined with ridges and dips within the same area. The final template has been converted to a master copy for nano-imprinting lithography of 3D fluidic structures and optical components. The process is scalable by allowing mask fabrication to mass produce structures over large areas, allowing integration of fine scale features with conventional wafer patterning technology.

Acknowledgements

We wish to thank the International Atomic Energy Agency for partial support under the CRP project number F11016. This work partly performed at SSLS under NUS Core

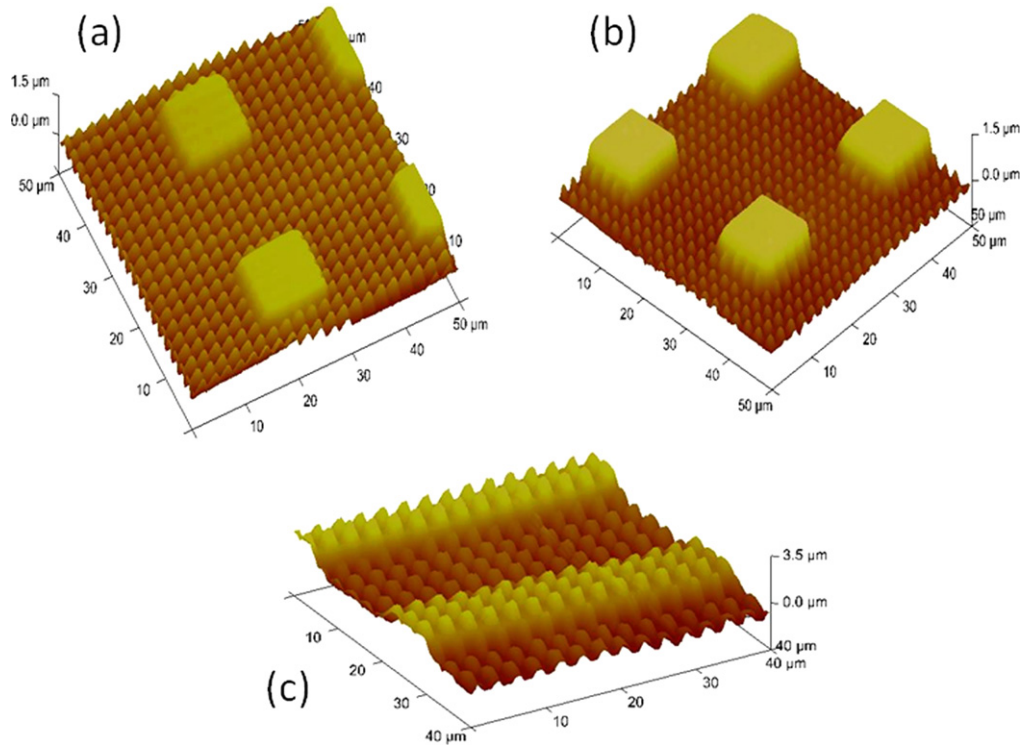

Figure 10. AFM images of a hierarchically patterned surface using 250 keV protons in (a), (b) 0.4 Ω cm and (c) 0.02 Ω cm silicon. After anodization at 60 mA cm^{-2} for (a), (b) 40 s and (c) 18 s the porous silicon was removed and the surface smoothed by oxidation at 1000 °C for 2 h.

Support C-380-003-003-001 and National Research Foundation project NRF-CRP8-2011-06.

References

[1] Cassie A B D and Baxter S 1944 Wettability of porous surfaces *Trans. Faraday Soc.* **40** 546–51
[2] Barthlott W and Neinhuis C 1997 Purity of the sacred lotus, or escape from contamination in biological surfaces *Planta* **202** 1–8
[3] Guo Z, Liu W and Su B-L 2011 Superhydrophobic surfaces: from natural to biomimetic to functional *J. Colloid Interface Sci.* **353** 335–55
[4] Kinoshita S, Yoshioka S and Miyazaki J 2008 Physics of structural colors *Rep. Prog. Phys.* **71** 076401
[5] Vasilev K, Cook J and Griesser H J 2009 Antibacterial surfaces for biomedical devices *Expert Rev. Med. Devices* **6** 553–67
[6] Pogodin S *et al* 2013 Biophysical model of bacterial cell interactions with nanopatterned cicada wing surfaces *Biophys. J.* **104** 835–40
[7] Kim P, Kreder M J, Alvarenga J and Aizenberg J 2013 Hierarchical or not? Effect of the length scale and hierarchy of the surface roughness on omniphobicity of lubricant-infused substrates *Nano Lett.* **13** 1793–9
[8] Dong C and Lei X X 2000 Biomechanics of cell rolling: shear flow, cell-surface adhesion, and cell deformability *J. Biomech.* **33** 35–43
[9] Stott S L *et al* 2010 Isolation of circulating tumor cells using a microvortex-generating herringbone-chip *Proc. Natl. Acad. Sci. USA* 1012539107
[10] Discher D E, Janmey P and Wang Y-l 2005 Tissue cells feel and respond to the stiffness of their substrate *Science* **310** 1139–43
[11] Tan J L, Tien J, Pirone D M, Gray D S, Bhadriraju K and Chen C S 2003 Cells lying on a bed of microneedles: an approach to isolate mechanical force *Proc. Natl. Acad. Sci. USA* **100** 1484–9
[12] Choi S and Park J-K 2008 Mirror-embedded microchannel for three-dimensional measurement of particle position *Appl. Phys. Lett.* **93** 191909
[13] Wang C and Zhang Y 2005 Protein micropatterning via self-assembly of nanoparticles *Adv. Mater.* **17** 150–3
[14] Boker A *et al* 2004 Hierarchical nanoparticle assemblies formed by decorating breath figures *Nat. Mater.* **3** 302–6
[15] Lee S K, Yi G R, moon J H, Yang S M and Pine D J 2006 Pixellated photonic crystal films by selective photopolymerization *Adv. Mater.* **18** 2111–6
[16] Zhang Y, Zha S and Liu M 2005 Dual-scale porous electrodes for solid oxide fuel cells from polymer foams *Adv. Mater.* **17** 487–91
[17] Autumn K, Liang Y A, Hsieh S T, Zesch W, Chan W P, Kenny T W, Fearing R and Full R J 2000 Adhesive force of a single gecko foot-hair *Nature* **405** 681–5
[18] Ball P 1999 Engineering shark skin and other solutions *Nature* **400** 507–9
[19] Zheng W, Zhang W and Jiang X 2013 Precise control of cell adhesion by combination of surface chemistry and soft lithography *Adv. Healthc. Mater.* **2** 95–108
[20] Qi H, Du Y, Wang L, Kaji H, Bae H and Khademhosseini A 2010 Patterned differentiation of individual embryoid bodies in spatially organized 3D hybrid microgels *Adv. Mater.* **22** 5276–81
[21] Chen Y-C, Lin R-Z, Qi H, Yang Y, Bae H, Melero-Martin J M and Khademhosseini A 2012 Functional human vascular network generated in photocrosslinkable gelatin methacrylate hydrogels *Adv. Funct. Mater.* **22** 2027–39

[22] Khademhosseini A, Vacanti J P and Langer R 2009 Progress in tissue engineering *Sci. Am.* **300** 64–71

[23] Klein F, Richter B, Striebel T, Franz C M, Freymann G V, Wegener M and Bastmeyer M 2011 Two-component polymer scaffolds for controlled three-dimensional cell culture *Adv. Mater.* **23** 1341–5

[24] Jeong K-H, Kim J and Lee L P 2006 Biologically inspired artificial compound eyes *Science* **312** 557–61

[25] Kobayashi K and Ikuta K 2008 Three-dimensional magnetic microstructures fabricated by microstereolithography *Appl. Phys. Lett.* **92** 262505

[26] Smart T, Lomas H, Massignani M, Flores-Merino M V, Perez L R and Battaglia G 2008 Block copolymer nanostructures *Nano Today* **3** 38–46

[27] Krishnamoorthy S, Manipaddy K K and Yap F L 2011 Wafer-level self-organized copolymer templates for nanolithography with sub-50 nm feature and spatial resolutions *Adv. Funct. Mater.* **21** 1102–12

[28] Bowen A M, Motala M J, Lucas J M, Gupta S, Baca A J, Mihi A, Alivisatos A P, Braun P V and Nuzzo R G 2012 Triangular elastomeric stamps for optical applications: near-field phase shift photolithography, 3D proximity field patterning, embossed antireflective coatings, and sers sensing *Adv. Funct. Mater.* **22** 2927–38

[29] Bita I, Choi T, Walsh M E, Smith H I and Thomas E L 2007 Large-area 3D nanostructures with octagonal quasicrystalline symmetry via phase-mask lithography *Adv. Mater.* **19** 1403–7

[30] Rogers J A, Paul K E, Jackman R J and Whitesides G M 1998 Generating; 90 nanometer features using near-field contact-mode photolithography with an elastomeric phase mask *J. Vac. Sci. Technol.* B **16** 59–68

[31] Wathuthanthri I, Liu Y, Du K, Xu W and Choi C-H 2013 Simple holographic patterning for high-aspect-ratio three-dimensional nanostructures with large coverage area *Adv. Funct. Mater.* **23** 608–18

[32] Jang J H, Ullal C K, Maldovan M, Gorishnyy T, Kooi S, Koh C and Thomas E L 2007 3D micro- and nanostructures via interference lithography *Adv. Funct. Mater.* **17** 3027–41

[33] Lin S Y, Fleming J G, Hetherington D L, Smith B K, Biswas R, Ho K M, Sigalas M M, Zubrzycki W, Kurtz S R and Bur J 1998 A three-dimensional photonic crystal operating at infrared wavelengths *Nature* **394** 251–3

[34] Fischer A C, Belova L M, Rikers Y G M, Gunnar Malm B, Radamson H H, Kolahdouz M, Gylfason K B, Stemme G and Niklaus F 2012 3D free-form patterning of silicon by ion implantation, silicon deposition, and selective silicon etching *Adv. Funct. Mater.* **22** 4004–8

[35] Livingston F E, Hansen W W, Huang A and Helvajian H 2002 Effect of laser parameters on the exposure and selective etch rate in photostructurable glass *Proc. SPIE* **4637** 404–12

[36] Maruo S, Nakamura O and Kawata S 1997 Three-dimensional microfabrication with two-photon-absorbed photopolymerization *Opt. Lett.* **22** 132–4

[37] Kawata S, Sun H-B, Tanaka T and Takada K 2001 Finer features for functional microdevices *Nature* **412** 697–8

[38] Cumpston B H *et al* 1999 Two-photon polymerization initiators for three-dimensional optical data storage and microfabrication *Nature* **398** 51–4

[39] Zhang Y-L, Chen Q-D, Xia H and Sun H-B 2010 Designable 3D nanofabrication by femtosecond laser direct writing *Nano Today* **5** 435–48

[40] Ovsianikov A, Mironov V, Stampfl J and Liska R 2012 Engineering 3D cell-culture matrices: multiphoton processing technologies for biological and tissue engineering applications *Expert Rev. Med. Devices* **9** 613–33

[41] Infuehr R, Pucher N, Heller C, Lichtenegger H, Liska R, Schmidt V, Kuna L, Haase A and Stampfl J 2007 Functional polymers by two-photon 3D lithography *Appl. Surf. Sci.* **254** 836–40

[42] Pina-Hernandez C, Guo L J and Fu P-F 2010 High-resolution functional epoxysilsesquioxane-based patterning layers for large-area nanoimprinting *ACS Nano* **4** 4776–84

[43] Ahn S H and Guo L J 2009 Large-area roll-to-roll and roll-to-plate nanoimprint lithography: a step toward high-throughput application of continuous nanoimprinting *ACS Nano* **3** 2304–10

[44] Pina-Hernandez C, Fu P-F and Guo L J 2011 Ultrasmall structure fabrication via a facile size modification of nanoimprinted functional silsesquioxane features *ACS Nano* **5** 923–31

[45] Aryal M, Trivedi K and Hu W 2009 Nano-confinement induced chain alignment in ordered P3HT nanostructures defined by nanoimprint lithography *ACS Nano* **3** 3085–90

[46] Glinsner T, Veres T, Kreindl G, Roy E, Morton K, Wieser T, Thanner C, Treiblmayr D, Miller R and Lindner P 2010 Fully automated hot embossing processes utilizing high resolution working stamps *J. Vac. Sci. Technol.* B **28** 36–41

[47] Matschuk M and Larsen N B 2013 Injection molding of high aspect ratio sub-100 nm nanostructures *J. Micromech. Microeng.* **23** 025003

[48] Nedelcu M, Saifullah M S M, Hasko D G, Jang A, Anderson D, Huck W T S, Jones G A C, Welland M E, Kang D J and Steiner U 2010 Fabrication of sub-10 nm metallic lines of low line-width roughness by hydrogen reduction of patterned metal–organic materials *Adv. Funct. Mater.* **20** 2317–23

[49] Huang X D, Bao L-R, Cheng X, Guo L J, Pang S W and Yee A F 2002 Reversal imprinting by transferring polymer from mold to substrate *J. Vac. Sci. Technol.* B **20** 2872–6

[50] Han K S, Hong S H, Kim K I, Cho J Y, Choi K W and Lee H 2013 Fabrication of 3D nano-structures using reverse imprint lithography *Nanotechnology* **24** 045304

[51] Aryal M, Ko D-H, Tumbleston J R, Gadisa A, Samulski E T and Lopez R 2012 Large area nanofabrication of butterfly wing's three dimensional ultrastructures *J. Vac. Sci. Technol.* B **30** 061802

[52] Schaper C D and Miahnahri A 2004 Polyvinyl alcohol templates for low cost, high resolution, complex printing *J. Vac. Sci. Technol.* B **22** 3323–6

[53] Park J, Fujita H and Kim B 2011 Fabrication of metallic microstructure on curved substrate by optical soft lithography and copper electroplating *Sensors Actuators* A **168** 105–11

[54] Svensson B G, Mohadjeri B, Hallén A, Svensson J H and Corbett J W 1991 Divacancy acceptor levels in ion-irradiated silicon *Phys. Rev.* B **43** 2292–8

[55] Anders H, Keskitalo N, Masszi F and Nágl V 1996 Lifetime in proton irradiated silicon *J. Appl. Phys.* **79** 3906

[56] Svensson B G, Jagadish C, Hallén A and Lalita J 1995 Point defects in MeV ion-implanted silicon studied by deep level transient spectroscopy *Nucl. Instrum. Methods Phys. Res.* B **106** 183–90

[57] Breese M B H, Grime G W and Dellith M 1993 The effect of ion induced damage on IBIC images *Nucl. Instrum. Methods Phys. Res.* B **77** 332–8

[58] Ziegler J F, Biersack J P and Littmark U 2003 *The Stopping and Range of Ions in Solids* (New York: Pergamon)

[59] Ziegler J F, Ziegler M D and Biersack J P 2010 SRIM—the stopping and range of ions in matter (2010) *Nucl. Instrum. Methods Phys. Res.* B **268** 1818–23

[60] Imai K 1981 A new dielectric isolation method using porous silicon *Solid-State Electron.* **24** 159–64

[61] Azimi S, Dang Z Y, Song J, Breese M B H, Vittone E and Forneris J 2013 Defect enhanced funneling of diffusion current in silicon *Appl. Phys. Lett.* **102** 042102

[62] Lehmann V 2002 *Electrochemistry of Silicon: Instrumentation, Science, Materials and Applications* (Weinheim: Wiley)
[63] Sailor M J 2011 *Porous Silicon in Practice: Preparation, Characterization and Applications* (Weinheim: Wiley)
[64] Azimi S, Breese M B H, Dang Z Y, Yan Y, Ow Y S and Bettiol A A 2012 Fabrication of complex curved three-dimensional silicon microstructures using ion irradiation *J. Micromech. Microeng.* **22** 015015
[65] Teo E J, Xiong B Q, Ow Y S, Breese M B H and Bettiol A A 2009 *Opt. Lett.* **34** 3142–4
[66] Azimi S, Song J, Dang Z Y, Liang H D and Breese M B H 2012 Three-dimensional silicon micromachining *J. Micromech. Microeng.* **22** 113001
[67] Dang Z Y, Song J, Azimi S, Breese M B H, Forneris J and Vittone E 2013 On the formation of silicon wires produced by high-energy ion irradiation *Nucl. Instrum. Methods Phys. Res.* B **296** 32–40
[68] Breese M B H, Grime G W and Watt F 1992 The nuclear microprobe *Annu. Rev. Nucl. Part. Sci.* **42** 1–38
[69] Mangaiyarkarasi D, Breese M B H, Ow Y S and Vijila C 2006 Controlled blueshift of the resonant wavelength in porous silicon microcavities using ion irradiation *Appl. Phys. Lett.* **89** 021910–3
[70] Mangaiyarkarasi D, Ow Y S, Breese M B H, Fuh V L and Xioasong E T 2008 Fabrication of large-area patterned porous silicon distributed Bragg reflectors *Opt. Express* **16** 12757–63
[71] Lai L and Irene E A 1999 Limiting Si/SiO_2 interface roughness resulting from thermal oxidation *J. Appl. Phys.* **86** 1729–35
[72] Lee K K, Lim D R, Kimerling L C, Shin J and Cerrina F 2001 Fabrication of ultralow-loss Si/SiO2 waveguides by roughness reduction *Opt. Lett.* **26** 1888–90